Fixed points and limit cycles in the population dynamics of lysogenic viruses and their hosts

Zhenyu Wang and Nigel Goldenfeld
Loomis Laboratory of Physics, Department of Physics, University of Illinois at Urbana–Champaign, 1110 West Green Street, Urbana, Illinois 61801, USA
and Institute for Genomic Biology, University of Illinois at Urbana–Champaign, 1206 West Gregory Drive, Urbana, Illinois 61801, USA
(Received 12 March 2010; published 22 July 2010)

Starting with stochastic rate equations for the fundamental interactions between microbes and their viruses, we derive a mean-field theory for the population dynamics of microbe-virus systems, including the effects of lysogeny. In the absence of lysogeny, our model is a generalization of that proposed phenomenologically by Weitz and Dushoff. In the presence of lysogeny, we analyze the possible states of the system, identifying a limit cycle, which we interpret physically. To test the robustness of our mean-field calculations to demographic fluctuations, we have compared our results with stochastic simulations using the Gillespie algorithm. Finally, we estimate the range of parameters that delineate the various steady states of our model.

DOI: 10.1103/PhysRevE.82.011918 PACS number(s): 87.23.Cc, 87.18.Tt, 87.18.Nq

I. INTRODUCTION

Microbes and their viruses are the most genetically diverse, abundant, and widely distributed organisms across the planet [1–4]. Microbes are major contributors to the global biogeochemical cycles and catalyze the reactions that have over evolutionary time brought the earth's surface to its present redox state [5]. Similarly, viruses, especially in the oceans, manipulate marine communities through predation and horizontal gene transfer [6,7], recycle nutrients, and thus drive the biological pump which leads *inter alia* to the sequestration of carbon in the deep ocean [8–17].

It is being increasingly realized that the classical view of microbial viruses purely as predators is too limited. Many microbe-virus interactions are lysogenic, not lytic: upon infection, the viral genetic material is incorporated into the chromosome of the host, replicates with the host, and can be subsequently released, typically triggered by the stress response of the host to environmental change [18]. As a result, viruses can transfer genes to and from bacteria, as well as being predators of them, so that the virosphere should properly be recognized as a massive gene reservoir [17,19–21]. Thus, there is a coevolution of both communities, the effects of which are complex and far reaching [10,17,20–25], even including the manipulation of bacterial mutation rates [26]. This nontrivial interaction between microbes and viruses has not gone unnoticed, with wide interest among biologists, ecologists, and geologists [2,18,25,27–34].

These findings highlight the importance of considering ecosystem dynamics within an evolutionary context. Conversely, evolution needs to be properly understood as arising from a spatially resolved ecological context, as was first recognized by Wallace over 150 years ago [35]. That speciation, and adaptation in general, arises at a particular point in time and space has a number of deep consequences that have not yet been incorporated into current theory. First, it means that evolutionary dynamics proceeds by the propagation of fronts, resulting in a complex and dynamical pattern of speciation, adaptation, and genome divergence that reflects its intrinsic dynamics and that of the heterogeneous and dynamical environment [36–39]. Second, as fronts expand, there are only a few pioneer organisms at the leading edge, and so demographic fluctuations are much larger than in the bulk. Such fluctuations profoundly influence the spatial structure of the populations, and during the last few years have been recognized to play a major role in population cycles [40] and even spatial pattern formation [41]. Third, the existence of horizontal gene transfer and genome rearrangement processes is strongly coupled to spatial distribution. For example, it is known that the probability of conjugation events is dependent on the local density, being essentially one per generation in closely packed biofilms, but an order of magnitude smaller in planktonic culture [42]. Moreover, the mechanism of horizontal gene transfer is also dependent on the density, with viral-mediated transduction being the most relevant mechanism at low density. How these patterns of evolutionary dynamics and species distribution play out is essentially unexplored. However, there have recently been the first reports of observations of the coupling between evolutionary and ecological time scales. In one such system (a predator-prey system realized in rotifer-algae interactions), it has been demonstrated that rapid evolutionary dynamics is responsible for the unusual phase-lag characteristics of the observed population oscillations [43]. Thus, rapid evolution is not only a major force for adaptation, but can have marked ecological consequences, too.

The complex interplay between evolution and the environment is nowhere more important than in early life, where the key questions concern how life emerged from abiotic geochemistry. Early life experienced demanding environments, whose closest modern day correspondence might be deep ocean hydrothermal vents or hot springs. It is known that there are high occurrences of lysogens in both environments [4,44], suggesting that microbe-phage interactions might also be important in the early stages of life, with lysogens playing an important role as a reservoir of genes and perhaps even aiding in the stabilization of early life populations through the limit cycle mechanism discussed in this paper.

Our goal in this paper is to lay a theoretical foundation for describing the interplay between ecology and evolution in

the context of microbe-virus systems, as these are arguably among the most important and probably the simplest of the complex systems in biology. The questions that will ultimately interest us are the evolutionary pressures that tune genetic switches governing the lysis-lysogeny decision, as well as the factors that shape prophage induction in response to environmental stress [45–47]. Such a foundation must begin with a proper account of the population dynamics itself, before coupling in detail to other levels of description involving genome dynamics, for example. Thus, we have chosen to focus in the present paper on the dynamics of microbe-virus systems, taking full account of both of the major viral pathways. In this paper, we are not specific about whether we are dealing with bacterial or archaeal viruses, but because most of the experiments to date are carried out on bacteria, we have tended to identify the microbes as bacteria and the viruses as phages, even though this is not required by the mathematics.

We are now ready to introduce the specific problem that we treat in this paper. Upon phage infection, there are two pathways awaiting the host bacterium [48]. In the first pathway—lysis—the bacteriophage produces a large number of copies of itself utilizing the bacterium's genetic material and molecular machinery. As a result, the bacterium ceases its metabolic function, and ruptures, releasing the newly assembled bacteriophage inside. The other pathway is lysogeny. In this process, the intruder integrates its own DNA into the genome of the bacterium, enters a dormant stage, and becomes a prophage. The infected bacterium is known as a lysogen—a relatively stable state [49], is immune to superinfection from the same or related strains, and is proceeding under normal replication life cycles. The DNA of the bacteriophage is duplicated, along with that of the host during cell replication. The lysogenic state can be terminated by environmental stress such as starvation, pollution, or ultraviolet irradiation, resulting in the process known as prophage induction: the exit of the prophage from the host genome and the subsequent lysis of the original bacterium and its bacterial descendants.

We now discuss briefly existing treatments of population dynamics in the context of microbe-virus systems. In 1977, Levin *et al.* [50] extended the celebrated Lotka-Volterra equations to model the dynamics between virulent phages and their victims, where only virulent phages are considered. A number of extensions have been proposed, extending the level of biological realism to include such features as the time delay arising between infection and lysis as well as the evolution of kinetic parameters [51–55]. In 2008, Weitz and Dushoff [56] proposed another way to improve the classic predator-prey model. Their attempt was mainly based on the experimental observation that the ability of a bacteriophage to lyse hosts degrades when the bacteria approach their carrying capacity [57–59]. Adding a new term to account for the saturation of the infection of the bacteriophages, they obtained an interesting phase diagram in which the fate of the bacteria-phage community can depend on the initial conditions. However, the new term is put in by hand, based on intuition which needs detailed mathematical support. Furthermore, they focused on virulent phages and excluded the temperate ones that elicit lysogeny, now regarded as essential to the survival of microbial communities through fluctuating environments [18,29,33].

These works are based on an ensemble-level description of the community, as in the classic work on predator-prey systems [60]. However, as is well known [60], the simplest of these models fails to capture the intrinsic cyclical behavior of predator-prey populations despite apparently incorporating fully the basic interactions that should give rise to cycles. This paradox was resolved by the important work of McKane and Newman [40], who showed that cyclical effects could only be captured at the level of an individual-level model and arose through the amplification of demographic noise. Their work showed how the conventional ensemble-level equations for predator-prey systems arose as the mean-field limit of the appropriate statistical field theory, with the essential effects of demographic noise entering the analysis as one-loop corrections to mean-field theory, in an inverse population size expansion. These effects can also be treated in a slightly more convenient formalism using path integrals [61]. The literature also does not have an explicit representation of lysogeny as it modifies the population dynamics of both host and phage.

The use of an individual-level model is important for a separate reason. By starting from microscopic rate processes, we can capture specific biological interactions and derive the corresponding mean-field population dynamics systematically. Such models are not always straightforward to write down phenomenologically, as shown by the fact that the equations assumed by Weitz and Dushoff [56] are not, as we show below, the most general form that takes into account the effects of host fitness on lysis.

The purpose of this paper is to provide a detailed theory of the population dynamics for host-phage communities. In contrast to earlier work, we pose the problem at the microscopic level, working with an individual-level model of bacteria and phage. From this fundamental description, we are able to derive the usual community-level description analogous to Lotka-Volterra equations from a mean-field theory. Our results encompass both virulent phages, such as those in Weitz and Dushoff's work [56], and lysogenic phages which have not been studied mathematically up to now.

This paper is organized as follows. In Sec. II, as a preliminary exercise, to present the technique, we treat a lysis-only model, in which we derive a set of dynamical equations roughly in the same form as in Weitz and Dushoff's paper [56] except for an additional parameter, which generally results in a relatively unimportant shift in the phase diagram. In the full lysogeny-lysis model, presented in Sec. III, we develop the formalism for the community of hosts and phages, including both lysis and lysogeny. Interestingly, we find that for certain combination of parameters, the community exhibits a limit cycle for all the species in the phase space, even at the level of mean-field theory. In order to interpret the corresponding range of parameters in a useful way for experimental observations, we map the parameters to rates in chemical reactions. In order to explore the robustness of our results, we demonstrate in Sec. IV that the corresponding limit cycle arises also in stochastic simulations with the Gillespie algorithm. Finally, in Sec. V we estimate the feasibility of verifying our predictions in laboratory experiments.

II. LYSIS-ONLY MODEL

A. Derivation of the population dynamics from an individual-level model

In this section, we adapt the classic predator-prey model to the host-phage communities from a microscopic or individual-level model. For simplicity, we first focus on two-component competition, where lysogens are excluded in spite of their biological importance. Hence, we are considering virulent phages and their hosts. Following the procedure given by McKane and Newman [40], we derive the population dynamics for the host-phage system, which Weitz and Dushoff [56] had written down phenomenologically. Here, we work at the level of mean-field theory, and we do not, in this paper, include the extension necessary for representing spatial degrees of freedom. Our individual-level model formalism is still needed, however, to systematically derive the population dynamics from the microscopic interactions. In our model, the host-phage dynamics differentiates itself from the classic predator-prey model in two ways: (1) only the host population is restricted by carrying capacity due to resource limitation and (2) the lysis of one host releases a particular number of phages (for example, about 100 replicates for lambda phage [48]), instead of only one predator in the classic predator-prey model. The above two points need to be accounted for carefully in the setup of the model, especially in the introduction and application of the carrying capacity, which will be explained explicitly as follows.

In our host-phage community, we have only one species of host and one species of phage which preys upon the former. Let us label the hosts by A and phages by B, whose populations are m and n, respectively. The hosts, either heterotrophic or autotrophic, need to consume environmental resources, which are renewable in every cycle, for survival and reproduction. All the environmental limitations on the hosts are abstracted into a maximal host population, which is denoted by the carrying capacity K. The phages, on the other hand, do not rely on the consumption of natural resources for maintenance once they are released into the environment. Thus, there is no such hard constraint on the phage population. Although phages are not restricted by K, we still introduce a virtual carrying capacity W for phages from dimensional considerations. It can be imagined that $W\to\infty$, so that no true carrying capacity is imposed on the phage population. The carrying capacities can be better visualized if we conceive space to be equally divided into K units for hosts and W units for phages. These units will be referred to as the host and phage layers, respectively. In the host layer, each unit is either occupied by one host or unoccupied, i.e., an empty site E. The total number of empty sites E is $K-m$. We construct the phage layer in a similar manner and denote the empty sites there by ϕ although the phage population is not confined actually. The population dynamics of the system can thus be modeled as arising from the following six microscopic events (Table I).

Here, b, c, d, e, f, and g are all constant rates. All the events above are written with constraints, with a nonlinear relation being incorporated automatically by adding empty sites E to the left of the arrows to reflect the restriction of carrying capacity K. For example, the birth of the host is density dependent, which needs an empty site to accommodate the newly born host. If no empty site is found, such an event cannot happen. Since we consider only the mean-field case, no spatial inhomogeneity is introduced. There is no concept of locality here, either. As long as an empty site is found, the newly born host is permitted. The crowding effect describes the competition in survival for limited natural resources among hosts. No such crowding effect exists for phages, which is in line with our assumption that there is no true carrying capacity confining the phage population. The two events in host-phage interaction are carefully chosen to give a minimal model while encompassing reduced lysis when the host population is approaching its carrying capacity. On the left-hand side of the arrows, we use "AE" and "AA" to label the good and poor metabolic statuses of the host, respectively. In this way, the effect of phage infection is entangled with the metabolism of its host. On the right-hand side of the arrows, α and β are the numbers of progeny for phage reproduction under good and poor metabolisms, respectively. There are two primary reasons which may account for the reduced lysis effect. The first is the decrease in the phage reproduction number [57], i.e.,

$$\alpha > \beta, \tag{1}$$

because phages need bacterial genetic materials, molecular machinery, and energy in the synthesis of their replicates. When the normal function of the host is downregulated, phage replication is correspondingly downshifted. The second reason is the reduced efficiency during phage infection, either in adsorption rates or viable infection, which leads to a diminishing of the infection cycle [57], i.e.,

$$e > f. \tag{2}$$

It might seem as if the model is discrete in the representation of metabolism since we put in good and poor metabolisms by hand. However, note that the actual metabolism of the community may be somewhere between good and poor, i.e., a linear combination, depending on the probability or fraction to enter either event. Hence, the separation of good and poor metabolisms is an essential part of our model, which

TABLE I. Microscopic events in the lysis-only model.

Description	Symbol
Birth of host	$AE \xrightarrow{b} AA$
Death of host due to longevity	$A \xrightarrow{c} E$
Death of host due to crowding effect	$AA \xrightarrow{d} AE$
Host-phage interaction:	
(i) under good metabolism	$AEB \xrightarrow{e} EE\alpha B$
(ii) under poor metabolism	$AAB \xrightarrow{f} EA\beta B$
Death of phage	$B \xrightarrow{g} \phi$

TABLE II. Probabilities for the combinations in the lysis-only model.

Combination	Probability
A	$\mu(1-\nu)\omega\frac{m}{K}$
AA	$\mu(1-\nu)(1-\omega)\frac{m(m-1)}{K(K-1)}$
AE	$\mu(1-\nu)(1-\omega)\frac{2m(K-m)}{K(K-1)}$
AEB	$\mu\nu(1-\omega)\frac{2m(K-m)}{K(K-1)}\frac{n}{W}$
AAB	$\mu\nu(1-\omega)\frac{m(m-1)}{K(K-1)}\frac{n}{W}$
B	$(1-\mu)\nu\frac{n}{W}$

yields the reduced lysis effect within the context of a minimal model. Finally, although phages do not age, their death can be induced by the rupture of capsids, and the corresponding rate is constant with time [62].

The time evolution of the whole community is accessed by random sampling. In each time step, we have a probability μ to draw units in the host layer and a probability ν to draw units in the phage layer. In the host layer, we may draw either one unit with probability ω or two units with probability $1-\omega$. In the phage layer, only one unit is drawn. If a combination not listed in Table I is drawn, such as *EEB*, nothing happens. Thus, all we need to consider are the above events. Using simple combinatorics, it is straightforward to obtain the probability for the combinations as follows from Table II where the factor of 2 accounts the equality in probability for events *AE* and *EA*, or *AEB* and *EAB*.

Thus, we obtain the transition matrices for each kind of variation in the population during each time step, such as $\langle T(m+1,n|m,n)\rangle$, and further the evolution for the probability in the population with m hosts and n phages at time t, $P(m,n,t)$. The reader is referred to Appendix A for calculational details.

The average of the population is given by summations

$$\langle m\rangle = \sum_{mn} mP(m,n,t), \tag{3a}$$

$$\langle n\rangle = \sum_{mn} nP(m,n,t). \tag{3b}$$

Thus, the time evolution for the population size is

$$\frac{d\langle m\rangle}{dt} = \langle T(m+1,n|m,n)\rangle - \langle T(m-1,n|m,n)\rangle - \langle T(m-1,n+\alpha-1|m,n)\rangle - \langle T(m-1,n+\beta-1|m,n)\rangle, \tag{4a}$$

$$\frac{d\langle n\rangle}{dt} = (\alpha-1)\langle T(m-1,n+\alpha-1|m,n)\rangle + (\beta-1)\langle T(m-1,n+\beta-1|m,n)\rangle - \langle T(m,n-1|m,n)\rangle. \tag{4b}$$

Here, we have taken the mean-field theory limit and neglected all the correlations and fluctuations.

Omitting angular brackets for simplicity, the equations for the evolution in population are

$$\frac{dm}{dt} = rm\left(1-\frac{m}{K}\right) - d_m m - \phi mn\left(1-a_m\frac{m}{K}\right), \tag{5a}$$

$$\frac{dn}{dt} = \gamma\phi mn\left(1-a_n\frac{m}{K}\right) - d_n n, \tag{5b}$$

where

$$r = \frac{(2b+d)\mu(1-\nu)(1-\omega)}{K}, \tag{6a}$$

$$\phi = \frac{2e\mu\nu(1-\omega)}{KW}, \tag{6b}$$

$$\gamma = \alpha - 1, \tag{6c}$$

$$d_m = \frac{[c\omega + d(1-\omega)]\mu(1-\nu)}{K}, \tag{6d}$$

$$d_n = \frac{(1-\mu)\nu}{W}, \tag{6e}$$

$$a_m = 1 - \frac{f}{2e}, \tag{6f}$$

$$a_n = 1 - \frac{\beta f}{2\alpha e}. \tag{6g}$$

Considering Eq. (1), we notice that Eqs. (6f) and (6g) yield the following relation:

$$0 < a_m < a_n < 1. \tag{7}$$

Generally speaking, $a_m \neq a_n$ unless

$$\alpha = \beta, \tag{8}$$

which implies that the reproduction numbers under good and poor metabolisms are the same as in Weitz and Dushoff's model. This concludes the derivation of the equations for population dynamics from the individual or microscopic level.

B. Results

In this section we explore the predictions of the lysis-only model given by Eq. (5). Let

$$t' = \frac{rt}{a_m}, \tag{9a}$$

$$\phi' = \frac{\phi\gamma K}{r}, \tag{9b}$$

$$d_n' = \frac{a_m d_n}{r}, \tag{9c}$$

$$d_m' = \frac{a_m d_m}{r} + 1 - a_m, \tag{9d}$$

$$m' = a_m \frac{m}{K}, \tag{9e}$$

$$n' = \frac{a_m n}{\gamma K}, \tag{9f}$$

$$a_n' = \frac{a_n}{a_m}. \tag{9g}$$

We can nondimensionalize the evolution equations (5). Omitting the primes we obtain

$$\frac{dm}{dt} = m(1-m) - \phi mn(1-m) - d_m m, \tag{10a}$$

$$\frac{dn}{dt} = \phi mn(1 - a_n m) - d_n n. \tag{10b}$$

Setting

$$\frac{dm}{dt} = 0, \tag{11a}$$

$$\frac{dn}{dt} = 0, \tag{11b}$$

we obtain three fixed points. The first is a trivial fixed point,

$$m = 0, \tag{12a}$$

$$n = 0, \tag{12b}$$

which is stable when

$$d_m > 1. \tag{13}$$

The second corresponds to the phage extinction phase

$$m = 1 - d_m, \tag{14a}$$

$$n = 0, \tag{14b}$$

which is stable when

$$0 < d_m < 1 - \frac{1}{a_n} \tag{15}$$

or

$$1 - \frac{1}{a_n} < d_m < 1, \tag{16}$$

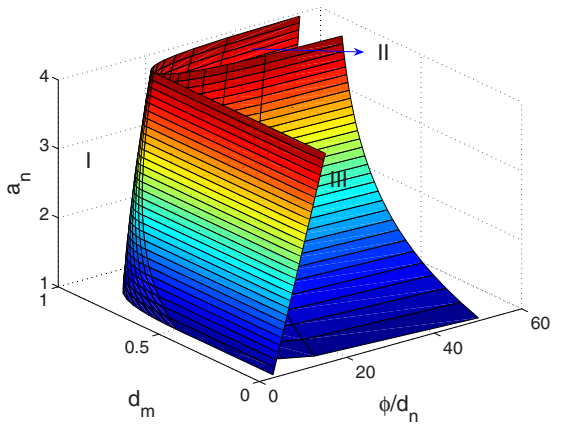

FIG. 1. (Color online) Three-dimensional phase diagram for the lysis-only model. Region I depends on the initial conditions to flow to the phage extinction or coexistence fixed point. Regions II and III are basins of attraction for coexistence and phage extinction fixed points, respectively.

$$\frac{\phi}{d_n} < \frac{1}{(1-d_m)[1 - a_n(1-d_m)]}. \tag{17}$$

The last is the coexistence of hosts and phages,

$$m = \rho, \tag{18a}$$

$$n = \frac{1}{\phi}\left(1 + \frac{d_m}{\rho - 1}\right), \tag{18b}$$

where ρ is a root of

$$a_n \phi \rho^2 - \phi\rho + d_n = 0. \tag{19}$$

The coexistence phase comes into existence and will be stable when

$$\frac{\phi}{d_n} \geq 4a_n, \tag{20}$$

$$d_m < 1 - \rho. \tag{21}$$

The stability of the fixed points is governed by the Jacobian

$$\begin{pmatrix} (1-2m)(1-\phi n) - d_m & -\phi m(1-m) \\ \phi n(1-2a_n m) & \phi m(1-a_n m) - d_n \end{pmatrix} \tag{22}$$

to the equations

$$m(1-m) - \phi mn(1-m) - d_m m = 0, \tag{23a}$$

$$\phi mn(1 - a_n m) - d_n n = 0. \tag{23b}$$

Thus, we obtain the three-dimensional phase diagram plotted in Fig. 1. The basin of attraction for the trivial case is not plotted. Region II is the basin of attraction for coexistence fixed point only while region III is that for the phage extinction. Region I will either go to coexistence or phage extinction, depending on the initial conditions.

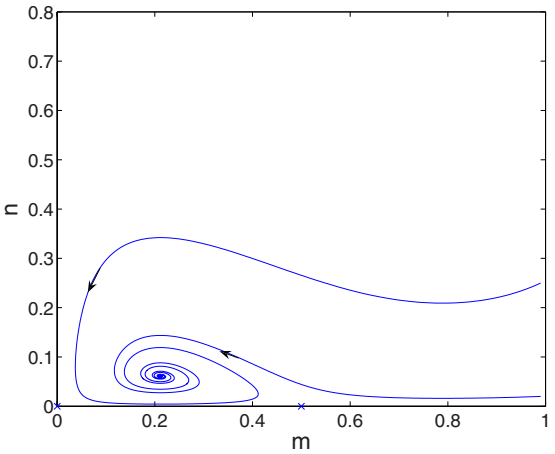

FIG. 2. (Color online) Flow diagram for $a_n=1$, $\phi=5$, $d_n=1$, and $d_m=0.1$. "×" denotes saddle points and "·" is for stable fixed points.

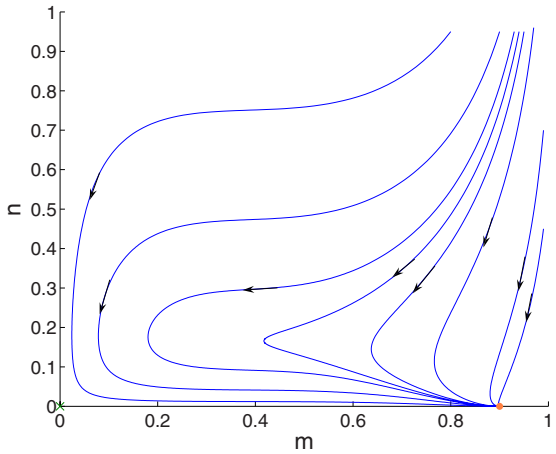

FIG. 3. (Color online) Flow diagram for $a_n=1.3$, $\phi=5$, $d_n=1$, and $d_m=0.1$. "×" denotes saddle points and "·" is for stable fixed points.

C. Discussion

As we can see, the bottom plane in Fig. 1 corresponds to the phase diagram in Weitz and Dushoff's model, where $a_n=1$. When

$$\alpha > \beta, \tag{24}$$

leading to

$$a_n > 1, \tag{25}$$

there is a shift in the phase diagram with a rapid shrinkage of the basin of attraction for region II, where any initial condition flows to the coexistence phase. The boundary between regions I and III also moves to larger ϕ/d_n, which implies that the more the good and poor metabolisms differ from each other in the progeny number, the easier the phages are driven out of the system. In order to see the effect of the phase shift more clearly, let us tune $a_n=1.3$ while keeping all the other parameters as those in Fig. 2(I) in Weitz and Dushoff's paper [56] (Fig. 2). When $a_n=1$, there is a neutral fixed point for coexistence. However, such a fixed point disappears (Fig. 3) when $a_n=1.3$. The flow diagrams are generated by fourth-order Runge-Kutta method.

In summary, we have obtained Weitz and Dushoff's model by detailed derivation from the individual or microscopic level and found a small shift in the phase diagram. Such a shift, as we see, can be observed experimentally by the onset of coexistence for the two species.

III. LYSOGENY-LYSIS MODEL

A. Derivation of the population dynamics from an individual-level model

In this section, we extend the lysis-only model above to incorporate lysogeny and investigate the important role of lysogeny in host-phage dynamics. Now there are three types of organism in the community. There are "healthy" hosts, which have no integration of phage genes, lysogens, and free phages, which live outside bacteria membranes. We will label healthy hosts, lysogens and free phages by A, D, and B, respectively, with population sizes m, s, and n. For the same reasons as in the lysis-only model, hosts and phages are thought of as being confined in different layers characterized by different carrying capacities. Hence both healthy hosts and lysogens are in the host layer with a total carrying capacity K. The empty sites in the host layer are denoted by E and their number is $K-m-s$. In the phage layer, the empty sites are labeled by ϕ as before.

The incorporation of lysogens brings us more microscopic events. There are two pathways after phage infections: lysis and lysogeny. Immediate lysis for temperate phages is the same process as for virulent ones, which has been characterized by events in the previous section. Lysogeny is an option only for temperate phages, which will be investigated in detail here. First, there should be an event corresponding to lysogen formation, i.e., a phage integrates its DNA into the genome of the host and turns itself into a prophage. Second, lysogens will survive, replicate, and die as healthy hosts. Last, environments might trigger prophage induction, which lyses the lysogen and releases the prophages inside. All in all, there are 18 microscopic events, which are listed in Table III.

Here, b, c, d, e, f, g, h, k, p, and q are constant reaction rates. α and β are phage reproduction numbers under good and poor metabolisms, respectively. Although prophage induction enhances the survival ability for lysogens in several ways, such as suppressing the latter's metabolism [18] through downregulation [63], for simplicity we have assumed the same birth and death rates for healthy hosts and lysogens. We have the condition

$$\alpha > \beta, \tag{26}$$

as before. Furthermore, there are the following advantages under better metabolism: more successful and effective infection [Eq. (27a)], greater possibility to lyse the host [Eq. (27b)], and faster prophage release [Eq. (27c)]. Since the mechanism for the lysis-lysogeny decision making of initial infection is different from the genetic switch for prophage induction [48,64], we do not expect any special relationship

TABLE III. Microscopic events in the lysogeny-lysis model.

Description	Symbol
Birth of host	$AE \xrightarrow{b} AA$
	$DE \xrightarrow{b} DD$
Death of host due to longevity	$A \xrightarrow{c} E$
	$D \xrightarrow{c} E$
Death of host due to crowding	$AA \xrightarrow{d} AE$
	$DD \xrightarrow{d} DE$
	$AD \xrightarrow{(1/2)d} DE$
	$AD \xrightarrow{(1/2)d} AE$
Host-phage interactions:	
(i) lysis under good metabolism	$AEB \xrightarrow{e} EE\alpha B$
(ii) lysis under poor metabolism	$AAB \xrightarrow{f} EA\beta B$
	$ADB \xrightarrow{f} ED\beta B$
(iii) lysogeny under good metabolism	$AEB \xrightarrow{h} DE$
(iv) lysogeny under poor metabolism	$AAB \xrightarrow{k} DA$
	$ADB \xrightarrow{k} DD$
Prophage induction:	
(i) under good metabolism	$DE \xrightarrow{p} EE\alpha B$
(ii) under poor metabolism	$DD \xrightarrow{q} DE\beta B$
	$DA \xrightarrow{q} AE\beta B$
Death of free phage	$B \xrightarrow{g} \phi$

between e and f, and p and q. These advantages can be expressed mathematically by the following inequalities:

$$e + h > f + k, \tag{27a}$$

$$\frac{e}{h} > \frac{f}{k}, \tag{27b}$$

$$p > q. \tag{27c}$$

We draw events from the two layers the same way as in the lysis-only model and this results in the probabilities shown in Table IV.

From these events, we obtain the following evolution equations for all the three species after the calculations provided in Appendix B:

TABLE IV. Probabilities for the combinations in the lysogeny-lysis model.

Combination	Probability
AE	$\mu(1-\nu)(1-\omega)\frac{2m(K-m-s)}{K(K-1)}$
DE	$\mu(1-\nu)(1-\omega)\frac{2s(K-m-s)}{K(K-1)}$
A	$\mu(1-\nu)\omega\frac{m}{K}$
D	$\mu(1-\nu)\omega\frac{s}{K}$
AA	$\mu(1-\nu)(1-\omega)\frac{m(m-1)}{K(K-1)}$
DD	$\mu(1-\nu)(1-\omega)\frac{s(s-1)}{K(K-1)}$
AD	$\mu(1-\nu)(1-\omega)\frac{2ms}{K(K-1)}$
AEB	$\mu\nu(1-\omega)\frac{2m(K-m-s)}{K(K-1)}\frac{n}{W}$
AAB	$\mu\nu(1-\omega)\frac{m(m-1)}{K(K-1)}\frac{n}{W}$
ADB	$\mu\nu(1-\omega)\frac{2ms}{K(K-1)}\frac{n}{W}$
B	$(1-\mu)\nu\frac{n}{W}$

$$\frac{dm}{dt} = rm\left(1 - \frac{m+s}{K}\right) - d_1 m - \phi_1 mn\left\{1 - \frac{1}{K}[(1-a_1)m + (1-2a_1)s]\right\}, \tag{28a}$$

$$\frac{ds}{dt} = rs\left(1 - \frac{m+s}{K}\right) - d_1 s + \phi_2 mn\left\{1 - \frac{1}{K}[(1-a_{21})m + (1-2a_{21})s]\right\} - d_2 s\left\{1 - \frac{1}{K}[(1-2a_{22})m + (1-a_{22})s]\right\}, \tag{28b}$$

$$\frac{dn}{dt} = [(\alpha-1)\phi_1 - \alpha\phi_2] \times mn\left\{1 - \frac{1}{K}[(1-a_{31})m + (1-2a_{31})s]\right\} + \alpha d_2 s\left\{1 - \frac{1}{K}[(1-2a_{32})m + (1-a_{32})s]\right\} - d_3 n, \tag{28c}$$

where

$$r = \frac{(2b+d)\mu(1-\nu)(1-\omega)}{K}, \tag{29a}$$

$$d_1 = \frac{[c\omega + d(1-\omega)]\mu(1-\nu)}{K}, \tag{29b}$$

$$d_2 = \frac{2p\mu(1-\nu)(1-\omega)}{K}, \tag{29c}$$

$$d_3 = \frac{(1-\mu)\nu}{W}, \tag{29d}$$

$$\phi_1 = \frac{2(e+h)\mu\nu(1-\omega)}{KW}, \tag{29e}$$

$$\phi_2 = \frac{2h\mu\nu(1-\omega)}{KW}, \tag{29f}$$

$$a_1 = \frac{f+k}{2(e+h)}, \tag{29g}$$

$$a_{21} = \frac{k}{2h}, \tag{29h}$$

$$a_{22} = \frac{q}{2p}, \tag{29i}$$

$$a_{31} = \frac{\beta f - k}{2(\alpha e - h)}, \tag{29j}$$

$$a_{32} = \frac{\beta q}{2\alpha p}. \tag{29k}$$

We note that

$$\phi_2 < \phi_1, \tag{30}$$

$$0 < a_1, a_{21}, a_{22}, a_{31}, a_{32} < 1, \tag{31}$$

$$a_{32} < a_{22}. \tag{32}$$

We also notice some kind of symmetry in the correction terms such as "$1-a_1$" and "$1-2a_1$." a_1 originates from the poor metabolism of hosts A, which indirectly downshifts the efficiency of phage infection and synthesis. In Eq. (28a), "a_1" comes from the event $AAB \xrightarrow{f} EA\beta B$, while "$2a_1$" is from $ADB \xrightarrow{f} ED\beta B$. The factor of "2" appears since "AD" is the same as "DA."

Considering

$$\alpha \gg 1, \tag{33}$$

for example,

$$\alpha \approx 100 \tag{34}$$

for lambda phage [48], we approximate

$$(\alpha - 1)\phi_1 - \alpha\phi_2 \approx \alpha(\phi_1 - \phi_2). \tag{35}$$

Hence Eq. (28c) can be simplified as

$$\frac{dn}{dt} = \alpha(\phi_1 - \phi_2)mn\left\{1 - \frac{1}{K}[(1-a_{31})m + (1-2a_{31})s]\right\} + \alpha d_2 s\left\{1 - \frac{1}{K}[(1-2a_{32})m + (1-a_{32})s]\right\} - d_3 n. \tag{36}$$

B. Results

In this section, we explore the predictions of the lysogeny-lysis model given by Eqs. (28a), (28b), and (36). Letting

$$t' = rt, \tag{37a}$$

$$\phi_1' = \frac{\alpha\phi_1 K}{r}, \tag{37b}$$

$$\phi_2' = \frac{\alpha\phi_2 K}{r}, \tag{37c}$$

$$d_1' = \frac{d_1}{r}, \tag{37d}$$

$$d_2' = \frac{d_2}{r}, \tag{37e}$$

$$d_3' = \frac{d_3}{r}, \tag{37f}$$

$$m' = \frac{m}{K}, \tag{37g}$$

$$s' = \frac{s}{K}, \tag{37h}$$

$$n' = \frac{n}{\alpha K}, \tag{37i}$$

and omitting the primes, the equations after nondimensionalization become

$$\frac{dm}{dt} = m(1-m-s) - d_1 m - \phi_1 mn[1-(1-a_1)m-(1-2a_1)s], \tag{38a}$$

$$\frac{ds}{dt} = s(1-m-s) - d_1 s + \phi_2 mn[1-(1-a_{21})m-(1-2a_{21})s] - d_2 s[1-(1-2a_{22})m-(1-a_{22})s], \tag{38b}$$

$$\frac{dn}{dt} = (\phi_1 - \phi_2)mn[1 - (1 - a_{31})m - (1 - 2a_{31})s]$$

$$+ d_2 s[1 - (1 - 2a_{32})m - (1 - a_{32})s] - d_3 n. \quad (38c)$$

Formally, the fixed points can be solved by requiring that

$$\frac{dm}{dt} = 0, \quad (39a)$$

$$\frac{ds}{dt} = 0, \quad (39b)$$

$$\frac{dn}{dt} = 0. \quad (39c)$$

However, we can only obtain four fixed points analytically. The first is the trivial case for the extinction of all the species,

$$m = 0, \quad (40a)$$

$$s = 0, \quad (40b)$$

$$n = 0. \quad (40c)$$

The second is the healthy host extinction fixed point,

$$m = 0, \quad (41a)$$

$$s = \frac{1 - d_1 - d_2}{1 - d_2(1 - a_{22})}, \quad (41b)$$

$$n = \frac{d_2}{d_3} s[1 - (1 - a_{32})s]. \quad (41c)$$

The third is the healthy host only fixed point,

$$m = 1 - d_1, \quad (42a)$$

$$s = 0, \quad (42b)$$

$$n = 0. \quad (42c)$$

The last is the lysogen extinction,

$$m = \frac{1}{1 - a_{21}}, \quad (43a)$$

$$s = 0, \quad (43b)$$

$$n = \frac{1 - m - d_1}{\phi_1[1 - (1 - a_1)m]}, \quad (43c)$$

whose existence requires that

$$(\phi_1 - \phi_2)(a_{31} - a_{21}) = d_3(1 - a_{21})^2. \quad (44)$$

The more interesting coexistence of all the three species is hard to solve analytically since the orders of the equations

$$m(1 - m - s) - d_1 m - \phi_1 mn[1 - (1 - a_1)m - (1 - 2a_1)s] = 0, \quad (45a)$$

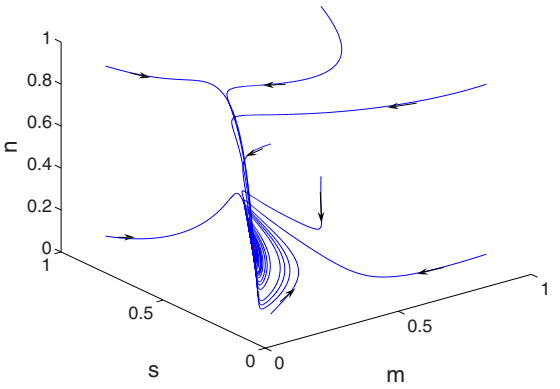

FIG. 4. (Color online) In the lysogeny-lysis model, a stable fixed point for the coexistence of all the three species. The parameters are $\phi_1=1$, $\phi_2=0.8$, $d_1=0.5$, $d_2=0.49$, $d_3=0.1$, $a_1=a_{21}=a_{31}=0.1$, and $a_{22}=a_{32}=0.5$.

$$s(1 - m - s) - d_1 s + \phi_2 mn[1 - (1 - a_{21})m - (1 - 2a_{21})s]$$

$$- d_2 s[1 - (1 - 2a_{22})m - (1 - a_{22})s] = 0, \quad (45b)$$

$$(\phi_1 - \phi_2)mn[1 - (1 - a_{31})m - (1 - 2a_{31})s]$$

$$+ d_2 s[1 - (1 - 2a_{32})m - (1 - a_{32})s] - d_3 n = 0 \quad (45c)$$

are too high. Using a fourth-order Runge-Kutta method, we found numerically a stable fixed point, shown in Fig. 4.

C. Discussion

As shown in Eqs. (38), there are, in total, ten parameters so that the phase space is difficult to visualize. We have studied the general trend of the transition between phases, starting with the dependence on phage mortality rate d_3. In Fig. 5, it is shown that when the phage mortality rate is low, the systems flow into a healthy host extinction phase. The phage population decreases with the increase in the phage mortality rate, which is very reasonable physically. For inter-

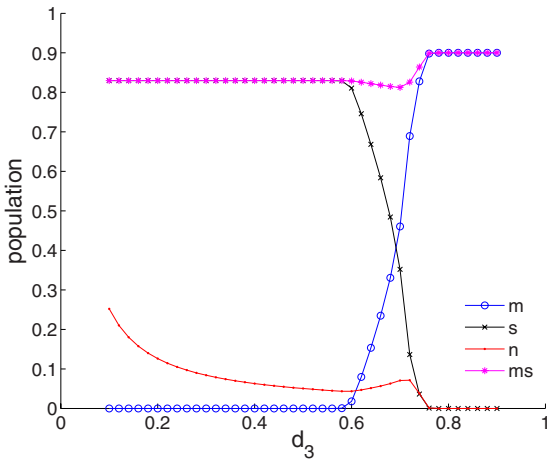

FIG. 5. (Color online) The population of the community with increasing phage mortality rate d_3. "*ms*" indicates the sum of m and s.

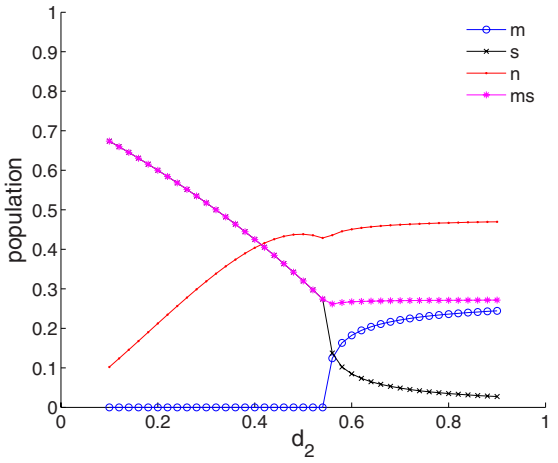

FIG. 6. (Color online) The population for the community with the increase in the lysis rate d_2.

mediate values of d_3, there is coexistence for all the three species, while for large values of d_3, the only survival is healthy host, where all phages die out quickly out, leading to the extinction of lysogens.

We show the trend of the population with increasing lysis rate d_2 in Fig. 6. The phage prospers with the increase in the lysis rate, while the lysogen diminishes. The peak in the phage population appears when there is a balance in the number of lysogens available to lyse and the lysis rate. When the lysis rate is beyond the threshold at 0.54, lysogen number falls dramatically and there is a proliferation of healthy hosts. The total host population is roughly the same afterward while the phage population upshifts a little with the increase in the healthy host available to infect, but does not change further when the ratio between healthy hosts and lysogens converges.

We have studied the effect of host mortality rate in Fig. 7. Obviously the total host population will fall monotonically when the hosts are more likely to die. We draw attention to the interesting peak in the phage population. When the host mortality rate is low, the phage population is suppressed due to the overcrowding of the lysogens, which degrades the metabolism and hence the infection and synthesis of phages. When the host mortality rate is high, on the other hand, the phages have insufficient hosts to infect and their population also declines.

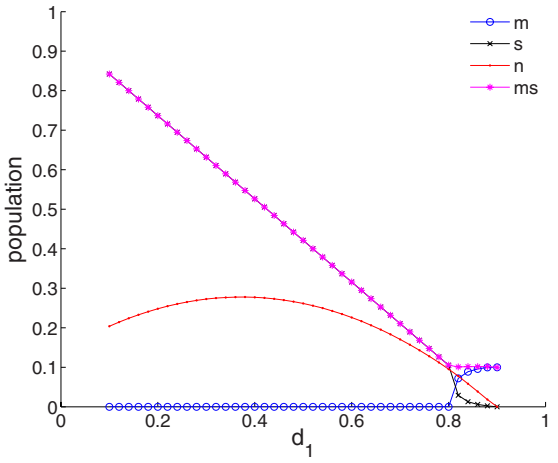

FIG. 7. (Color online) The population for the community with the increase in the host mortality rate d_1.

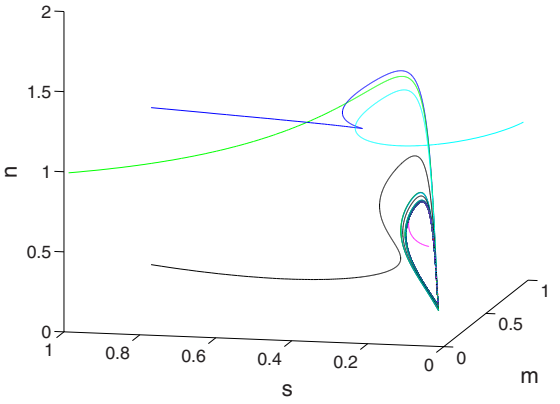

FIG. 8. (Color online) A limit cycle in the flow diagram for different initial conditions with parameters $\phi_1=1$, $\phi_2=0.8$, $d_1=0.5$, $d_2=0.49$, $d_3=0.03$, $a_1=a_{21}=a_{31}=0.1$, and $a_{22}=a_{32}=0.5$.

D. Existence of a limit cycle

We have noticed that the dynamics exhibits a limit cycle [65,66] for some combination of parameters (Fig. 8). In this section, we describe our numerical evidence for this assertion and present a plausible physical interpretation of our finding. In order to verify that it is a limit cycle instead of some unexpected slowing down near a putative stable or neutral fixed point, we have chosen an initial condition located inside the conjectured limit cycle. If there is, in fact, no real limit cycle, the dynamics will flow inward no matter how slow it will be. However, as we can see in Fig. 9, the trajectory indicated by the red (light gray) curve flows out.

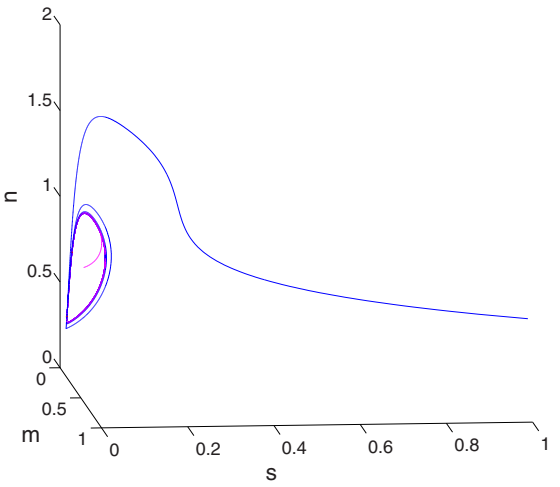

FIG. 9. (Color online) A limit cycle in the flow diagram with different initial conditions for parameters $\phi_1=1$, $\phi_2=0.8$, $d_1=0.5$, $d_2=0.49$, $d_3=0.03$, $a_1=a_{21}=a_{31}=0.1$, and $a_{22}=a_{32}=0.5$. The limit cycle is in a curved space. The blue (black) curve initiated outside the cycle flows in, while the red (light gray) one from inside flows out.

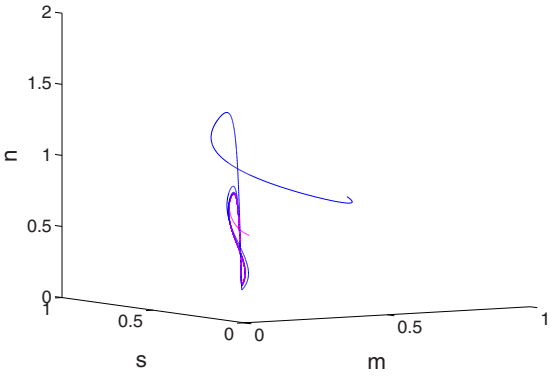

FIG. 10. (Color online) A limit cycle in the flow diagram with different initial conditions for parameters $\phi_1=1$, $\phi_2=0.8$, $d_1=0.5$, $d_2=0.49$, $d_3=0.03$, $a_1=a_{21}=a_{31}=0.1$, and $a_{22}=a_{32}=0.5$. The limit cycle is in a curved space.

Hence we have observed in the flow diagram an oscillation in the population for all the three species. If we inspect neighboring time steps, it appears that the convergence is slow since the deviation from step to step is very small. However, on longer time scales, we can see that the convergence is an illusion. Moreover, tilting the view angle, we see that the limit cycle is in some curved space instead of a single plane in Fig. 10. In order to investigate the emergence of the limit cycle, we have scanned part of the parameter space. For example, there is a stable coexistence fixed point for $d_1>0.41$ while $\phi_1=1$, $\phi_2=0.8$, $d_2=0.9$, $d_3=0.048$, $a_1=a_{21}=a_{31}=0.1$, and $a_{22}=a_{32}=0.5$. However, the above fixed point becomes unstable if $d_1<0.41$ leading to the limit cycle. As we see it, such an oscillation of the population in the community is a manifestation of the role of lysogens (Fig. 11). When the populations for hosts and phages are both small, the host will enjoy a boom because of good metabolism and little phage infection. Meanwhile prophages replicate with the fast reproduction of lysogens. Once the lysogeny-lysis switch is triggered, the destruction of lysogens will yield a huge virus burst. Then healthy host will encounter intensive phage infection and hence be suppressed. When most of the hosts die out, phage population shrinks quickly due to lack of infection. In this way, a cycle forms. Integrating its DNA into the genome of a lysogen, a prophage is sheltered although it is temporarily dormant in the sense of viral infection. Such a stage assists prophages to survive demanding environmental conditions and provides an opportunity to resurrect the population when there are abundant healthy hosts. Thus, lysogens are perfect genetic reservoirs for phages for potential future burst [18,21].

IV. STOCHASTIC SIMULATION

Up to now, all the calculations above were carried out within the scope of mean-field theory. As a next step, it is important to see to what extent such predictions are disturbed by demographic fluctuations, and especially whether the limit cycle in the lysogeny-lysis model is stable. A second goal of this section is to link the parameters the parameters in our model to those which could characterize real experiments. In this section, we perform stochastic simulations using the Gillespie's algorithm [67,68], which is a very efficient strategy to simulate chemical reactions. The reaction rates (b, c, d, e, f, and g in Table I; and b, c, d, e, f, g, h, k, p, and q in Table III) are interpreted as average probability rates for the occurrence of the corresponding reactions in line with the Gillespie algorithm, where the effect of draw probability is incorporated automatically.

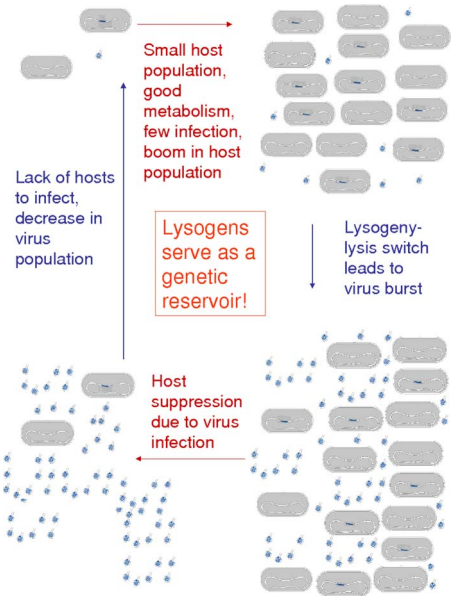

FIG. 11. (Color online) Cartoon explanation for the limit cycle. When the populations for hosts and phages are both small, the host will enjoy a boom because of good metabolism and little phage infection. Meanwhile prophages replicate with the fast reproduction of lysogens. Once the lysogeny-lysis switch is triggered, the destruction of lysogens will yield a huge virus burst. Then healthy host will encounter intensive phage infection and hence be suppressed. When most of the hosts die out, phage population shrinks quickly due to lack of infection. In this way, a cycle forms.

In the lysis-only model, the map between the two sets of parameters for reactions is

$$\tilde{b} = bK, \tag{46a}$$

$$\tilde{c} = c, \tag{46b}$$

$$\tilde{d} = \tfrac{1}{2}dK, \tag{46c}$$

$$\tilde{e} = eK, \tag{46d}$$

$$\tilde{f} = \tfrac{1}{2}fK, \tag{46e}$$

$$\tilde{g} = g, \tag{46f}$$

where overtilde is used to indicate the probability rates in the Gillespie algorithm. Since there are more degrees of freedom in choosing microscopic event rates, different stochastic simulations may map into the same mean-field phase diagram.

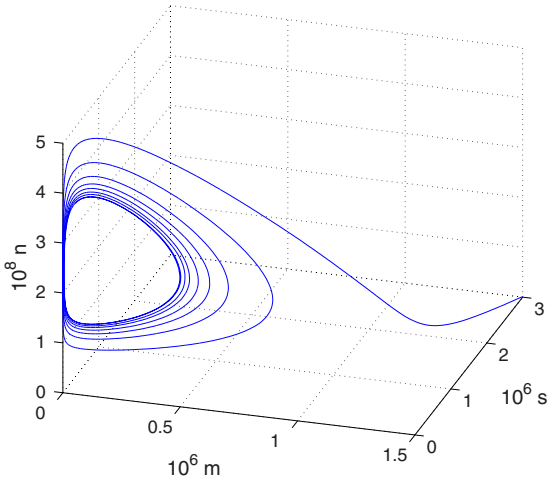

FIG. 12. (Color online) A limit cycle in the phase space with parameters in the Gillespie algorithm $\tilde{b}=0.4$, $\tilde{c}=0.1$, $\tilde{d}=0.2$, $\tilde{e}=1.2\times10^{-10}$, $\tilde{f}=1.2\times10^{-11}$, $\tilde{g}=0.018$, $\tilde{h}=4.8\times10^{-10}$, $\tilde{k}=4.8\times10^{-11}$, $\tilde{p}=0.54$, and $\tilde{q}=0.27$.

Our main interest is to explore the mean-field limit cycle in the lysogeny-lysis model. We keep employing the overtilde symbol to label the probability rates in the Gillespie sense and the map is

$$\tilde{b} = bK, \tag{47a}$$

$$\tilde{c} = c, \tag{47b}$$

$$\tilde{d} = \tfrac{1}{2}dK, \tag{47c}$$

$$\tilde{e} = eK, \tag{47d}$$

$$\tilde{f} = \tfrac{1}{2}fK, \tag{47e}$$

$$\tilde{h} = hK, \tag{47f}$$

$$\tilde{k} = \tfrac{1}{2}kK, \tag{47g}$$

$$\tilde{p} = pK, \tag{47h}$$

$$\tilde{q} = \tfrac{1}{2}qK, \tag{47i}$$

$$\tilde{g} = g. \tag{47j}$$

In Fig. 12, we show a limit cycle observed in our stochastic simulations. It is broadly consistent with the mean-field predictions, as can be noted easily by the obvious similarities between Figs. 13 and 14, and Figs. 15 and 16 (when we project the three-dimensional phase space onto two dimensions), whose relationship is Eqs. (37g)–(37i). As expected, we notice fluctuations in the stochastic simulation. For example, if Fig. 12 were shown in better resolution, we can see that the curve fluctuates slightly around the limit cycle. Usually the fluctuation is two orders of magnitude smaller than

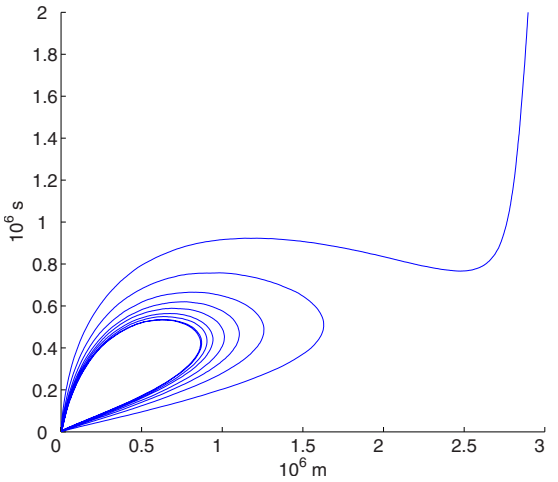

FIG. 13. (Color online) The projection of Fig. 12 onto the *m*-*s* plane.

the mean value. In order to explore the robustness of the limit cycle, we ran extensive tests to try and estimate their lifetime. As an example, for a given set of mean-field parameters that yield the limit cycle, we varied d_1, mapped the model onto the corresponding parameters for a stochastic simulation, and then ran simulations for 10^{10} time steps each with five sets of different initial conditions. As long as the carrying capacity K was large enough (above 10^7), we were unable to observe any disappearance of the limit cycle within the duration of our simulation. Furthermore, all simulations flowed into the same limit cycle.

In general terms, there is the following intuition about the conditions under which the limit cycle is robust: if the viral burst from lysogens is too big, it will drive healthy hosts to extinction. If the burst is too small, it will lose control over the population of the healthy hosts. In either case, the limit cycle will fail to form or become unstable. Hence, we conclude that the limit cycle is inherent to the model and robust to stochastic fluctuations, which serves to confirm the essential role of lysogens in stabilizing the cycling in the populations.

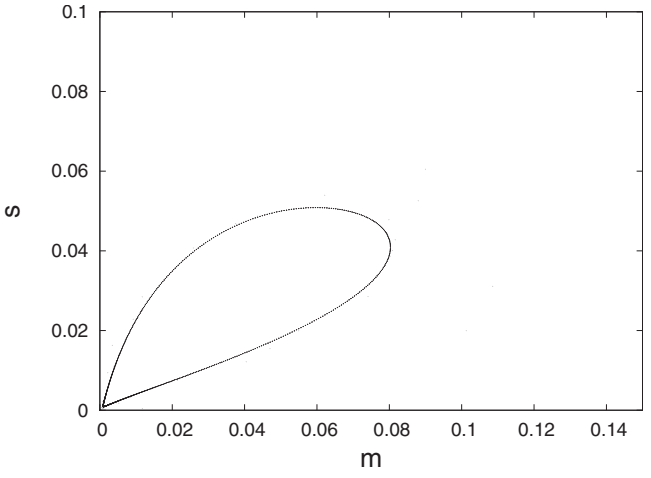

FIG. 14. A limit cycle projected onto *m*-*s* plane in the mean-field theory with parameters $\phi_1=1$, $\phi_2=0.8$, $d_1=0.5$, $d_2=0.9$, $d_3=0.03$, $a_1=a_{21}=a_{31}=0.1$, and $a_{22}=a_{32}=0.5$.

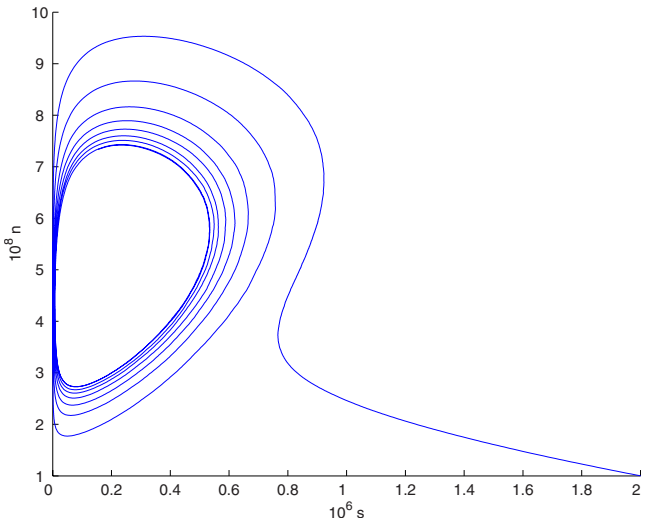

FIG. 15. (Color online) The projection of Fig. 12 onto the *s*-*n* plane.

V. PARAMETERS IN THE MODEL

Up to this point, all the parameters above or their values we have explored are difficult to relate to experiment. The purpose of this section is to bridge the gap.

The birth rate of the host b is medium dependent. Usually the expression of Lac proteins is highly suppressed by Lac repressors in a lacose-free medium to optimize energy investment and metabolism of the bacteria. In the above two models, we have categorized the death of the hosts to longevity and crowding. In fact, it is hard to mark a watershed clearly. Instead, what is observed is a population-dependent growth rate, which is a combined effect of b, c, and d. Herein, the rate d for the death of the host due to crowding is introduced artificially to account for the actual population dependence. Thus, we are justified in assuming that the death rate of the host due to longevity c, which incorporates other physical and non-density-dependent factors, is fixed with the

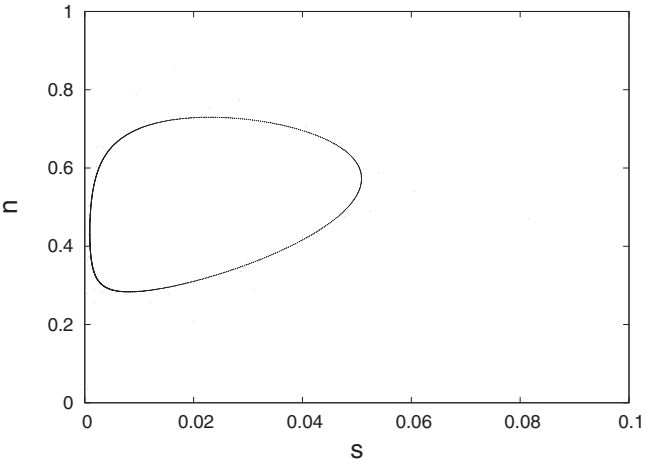

FIG. 16. A limit cycle projected onto the *s*-*n* plane in the mean-field theory with parameters $\phi_1=1$, $\phi_2=0.8$, $d_1=0.5$, $d_2=0.9$, $d_3=0.03$, $a_1=a_{21}=a_{31}=0.1$, and $a_{22}=a_{32}=0.5$.

variation in host population. The growth rate for *E. coli* may drop to 0.2 h^{-1} at 37 °C when glycolate serves as the carbon source but usually is in the range from 0.5 to 2.0 h^{-1} [27,69]. The growth rate is species and strain specific, which for *Pseudoalteromonas sp.* strain SKA18 (accessible number AF188330 in GenBank) [57], for example, is an order of magnitude smaller. Similarly, the lysis rate f, lysogeny rate k, prophage induction rate q, and replicate number per capita β, which are all under poor metabolism, are introduced manually to characterize the population-dependent feature of the interactions in order to leave their population-independent counterparts e, h, p, and α fixed. In the case of virulent phages, such as the one in the family *Siphoviridae* [70] attacking *Pseudoalteromonas sp.* strain SKA18 [57], corresponding to the lysis-only model, the reported lysis rate spans from 0.2 to 2.0 h^{-1} subject to the growth rate of the bacteria, so that we can estimate e to be on the order of 1.0 h^{-1} and f to be an order of magnitude smaller than e.

For temperate phages in the lysogeny-lysis model, the spontaneous lysis rate is far smaller, being on the order of 10^{-9}–10^{-7} per generation per cell [71]. The percentage of lysogens is assayed through prophage induction by the addition of mitomycin C, uv radiation, or other environmental conditions that may inhibit lambda phage repressors. Under good metabolism the lysogeny rate h for λ phage infecting *E. coli* and prophage induction rate are on the order of 1 and 2 h^{-1}, respectively [72]. Their counterparts under poor metabolism are estimated to be one or two orders of magnitude smaller. For instance, the prophage induction rate for log-phase marine lysogens [73] is on the order of 0.03 h^{-1}. Replicate number per capita α is about 100 for phage λ [48], and may be up to 600 for phage W-14 [74], while β is about 20 or 30 for both. Although virions do not age [62], their mortality is caused by the destabilization of the capsid, which is dependent on physical conditions such as temperature, humidity and pH values. Jepson and March [75] reported that phage λ is highly stable, whose half life in suspension ranges from 2.3 days at 4.2 °C to 36 days at 20 °C. Even if we take the half life be 1 day, the corresponding death rate g is on the order of 10^{-6}/s and can be suppressed by cooling down. Actually, the loss of free phage in nature, to a great extent, is through diffusion since bacteria are more immobile due to their large particle size compared to that of phages. In laboratory, the death rate can be manipulated through continuous dilution and washing out, and a wide range of death rates can be realized.

When all the parameters are tuned properly, the limit cycle in the lysogeny-lysis model is observable in experiment. We estimate the period of the limit cycle to be on the order of days, and thus in principle observable in laboratory experiments. For example, consider Fig. 13. A cycle there is composed of about 10 000 computational steps, in other words 10 000 events, which corresponds to about 120 [time units] in the simulation. In Fig. 13 the birth rate is 0.6 [time units]$^{-1}$, while in the real world the life cycle of an *E. coli* in good laboratory conditions, for example, is about half an hour, which is 2 h^{-1}. Hence the cycle is $120\times0.6/2=36$ h, which is 1 and 1/2 day. When we vary

parameters in the Gillespie algorithm, as long as they map to the same limit cycle in the mean-field theory, the period stays the same. The period will change only when it corresponds to different limit cycles in the mean-field sense. When we increase d_1' from 0.32 to 0.41 in the mean-field theory, the period may drop from 36 to 28 h at the edge of the disappearance of the limit cycle.

VI. CONCLUSION

We have derived the mean-field population dynamics for host-phage communities both without and with lysogens. In the lysis-only model, we successfully obtained a description similar to the starting point assumed by Weitz and Dushoff [56], and we found that the phase diagram was modified only slightly to the difference in good and poor metabolisms. In the lysogeny-lysis model, we identified the asymptotic states, which included not only coexistence and extinction fixed points, but population cycling of all microbes, lysogens, and phages. Our findings support the notion that lysogens act as a reservoir and are in principle amenable to experimental verification. We simulated the stochastic process using the Gillespie algorithm and verified the robustness of our results to fluctuations, and especially demonstrated the stability of the limit cycle.

Although complicated, our model inevitably makes some drastic assumptions, among which the most severe is the omission of spatial structure. Discreteness in the occurrence of speciation and adaptation in time and space may have a complex interplay with spatial heterogeneity since it propagates with large fluctuations at fronts [36–39]. Such demographic noise may also induce robust spatial patterns beyond mean-field predictions [41]. Hence, inclusion of spatial structure may yield interesting predictions about the spatial structure of microbe-virus communities, with concomitant consequences for the evolutionary dynamics, too. Another simplification is that we treat healthy hosts and lysogens in the same way regarding their natural birth, death, and crowding effect. However, experimentally, the expression of prophage genes and the control of host gene expression by viral genes seem to impart to lysogens economization in their metabolism [18]. When unnecessary metabolic activities are suppressed, lysogens optimize their energy expenses and therefore gain some survival advantage compared to healthy hosts in unfavorable conditions, which suggests that the natural birth, death, and crowding effects of lysogens are distinct from those of healthy hosts. Hence, our model is a reasonable minimal model that can capture the nontrivial role of lysogens in the population dynamics of microbe-phage communities, in addition to the usual predator-prey interactions, but more biological realism could be introduced.

This work can be extended in several ways, but perhaps the most interesting are those which relate to the evolution of the field of genes distributed among the microbes, viruses, and lysogens. Lysogens are genome carriers of not only microbes but also prophages, capable of yielding virus bursts when triggered by environmental stress. In this way, the role of lysogens and viruses as a reservoir of genes is mediated through phage infection and the lysogeny-lysis switch by the metabolism of the host. The metabolism of the host is, in turn, to a great extent influenced by environmental conditions. Thus, this model is a starting point for ecology-mediated evolution. It is also useful to stress that each individual microbe or virus constitutes a part of another organism's environment. Thus, the effects which our work begins to treat represent a microcosm of the intricate interplay between ecology and evolution in microbe-virus communities.

ACKNOWLEDGMENTS

We are grateful to Carl Woese, Ido Golding, Rachel Whitaker, Nicholas Chia, David Reynolds, Nicholas Guttenberg, Patricio Jeraldo, Tom Butler, and Maksim Sipos for helpful discussions. We thank Joshua Weitz for helpful comments on an earlier version of this paper. This work was supported in part by the National Science Foundation through Grant No. NSF-0526747.

APPENDIX A: TRANSITION MATRICES FOR THE LYSIS-ONLY MODEL

Here, we provide the transition matrices, which are the probabilities for the change in the population in each time step in the lysis-only model,

$$T(m+1,n|m,n) = b\mu(1-\nu)(1-\omega)\frac{2m(K-m)}{K(K-1)} = \tilde{b}m\left(1-\frac{m}{K}\right), \tag{A1}$$

$$\tilde{b} = \frac{2b\mu(1-\nu)(1-\omega)}{K-1} \approx \frac{2b\mu(1-\nu)(1-\omega)}{K}, \tag{A2}$$

$$T(m-1,n|m,n) = c\mu(1-\nu)\omega\frac{m}{K} + d\mu(1-\nu)(1-\omega)\frac{m(m-1)}{K(K-1)} = \tilde{c}m + \tilde{d}m\left(\frac{m}{K}-\frac{1}{K}\right) \approx \tilde{c}m + \tilde{d}\frac{m^2}{K}, \tag{A3}$$

$$\tilde{c} = \frac{c\mu(1-\nu)\omega}{K}, \tag{A4}$$

$$\tilde{d} = \frac{d\mu(1-\nu)(1-\omega)}{K-1} \approx \frac{d\mu(1-\nu)(1-\omega)}{K}, \tag{A5}$$

$$T(m-1,n+\alpha-1|m,n) = e\mu\nu(1-\omega)\frac{2m(K-m)}{K(K-1)}\frac{n}{W} = \tilde{e}mn\left(1-\frac{m}{K}\right), \tag{A6}$$

$$\tilde{e} = \frac{2e\mu\nu(1-\omega)}{(K-1)W} \approx \frac{2e\mu\nu(1-\omega)}{KW}, \tag{A7}$$

$$T(m-1,n+\beta-1|m,n) = f\mu\nu(1-\omega)\frac{m(m-1)}{K(K-1)}\frac{n}{W} = \tilde{f}\frac{m^2 n}{K}, \tag{A8}$$

$$\tilde{f} = \frac{f\mu\nu(1-\omega)}{(K-1)W} \approx \frac{f\mu\nu(1-\omega)}{KW}, \tag{A9}$$

$$T(m,n-1|m,n) = g(1-\mu)\nu\frac{n}{W} = \tilde{g}n, \tag{A10}$$

$$\tilde{g} = \frac{(1-\mu)\nu}{W}. \tag{A11}$$

All the other transition matrices are zero. Noting that all the events in Table I are Markovian processes, we know that the time evolution for the probability with m hosts and n phages at time t will be

$$\begin{aligned}\frac{d}{dt}P(m,n,t) &= T(m,n|m-1,n)P(m-1,n,t) + T(m,n|m+1,n)P(m+1,n,t) + T(m,n|m+1,n+\alpha-1)P(m+1,n+\alpha-1,t)\\ &+ T(m,n|m+1,n+\beta-1)P(m+1,n+\beta-1,t) + T(m,n|m,n+1)P(m,n+1,t) - [T(m+1,n|m,n)\\ &+ T(m-1,n|m,n) + T(m-1,n+\alpha-1|m,n) + T(m-1,n+\beta-1|m,n) + T(m,n-1|m,n)]P(m-1,n,t).\end{aligned} \tag{A12}$$

Applying summations according to Eqs. (3), we will get

$$\begin{aligned}\frac{d\langle m\rangle}{dt} &= \langle T(m+1,n|m,n)\rangle - \langle T(m-1,n|m,n)\rangle - \langle T(m-1,n+\alpha-1|m,n)\rangle - \langle T(m-1,n+\beta-1|m,n)\rangle\\ &\approx (\tilde{b}+\tilde{d})\langle m\rangle\left(1-\frac{\langle m\rangle}{K}\right) - (\tilde{c}+\tilde{d})\langle m\rangle - \tilde{e}\langle m\rangle\langle n\rangle\left[1-\left(1-\frac{\tilde{f}}{\tilde{e}}\right)\frac{\langle m\rangle}{K}\right],\end{aligned} \tag{A13a}$$

$$\begin{aligned}\frac{d\langle n\rangle}{dt} &= (\alpha-1)\langle T(m-1,n+\alpha-1|m,n)\rangle + (\beta-1)\langle T(m-1,n+\beta-1|m,n)\rangle - \langle T(m,n-1|m,n)\rangle\\ &= (\alpha-1)\tilde{e}\langle m\rangle\langle n\rangle\left[1-\left(1-\frac{(\beta-1)\tilde{f}}{(\alpha-1)\tilde{e}}\right)\frac{\langle m\rangle}{K}\right] - \tilde{g}\langle n\rangle.\end{aligned} \tag{A13b}$$

Letting

$$r = \tilde{b} + \tilde{d}, \tag{A14a}$$

$$\phi = \tilde{e}, \tag{A14b}$$

$$\gamma = \alpha - 1, \tag{A14c}$$

$$d_m = \tilde{c} + \tilde{d}, \tag{A14d}$$

$$d_n = \tilde{g}, \tag{A14e}$$

$$a_m = 1 - \frac{\tilde{f}}{\tilde{e}}, \tag{A14f}$$

$$a_n = 1 - \frac{(\beta-1)\tilde{f}}{(\alpha-1)\tilde{e}}, \tag{A14g}$$

which are Eqs. (6), we can arrive at Eqs. (5).

APPENDIX B: TRANSITION MATRICES FOR THE LYSOGENY-LYSIS MODEL

In this appendix, we provide details for the derivations of the lysogeny-lysis model. According to Tables III and IV, we can obtain the following nonzero transition matrices:

$$\begin{aligned}T(m+1,s,n|m,s,n) &= b\mu(1-\nu)(1-\omega)\frac{2m(K-m-s)}{K(K-1)}\\ &= \tilde{b}m\left(1-\frac{m+s}{K}\right),\end{aligned} \tag{B1}$$

$$\tilde{b} = \frac{2b\mu(1-\nu)(1-\omega)}{K-1} \approx \frac{2b\mu(1-\nu)(1-\omega)}{K}, \tag{B2}$$

$$T(m,s+1,n|m,s,n) = b\mu(1-\nu)(1-\omega)\frac{2s(K-m-s)}{K(K-1)} = \tilde{b}s\left(1-\frac{m+s}{K}\right), \tag{B3}$$

$$\begin{aligned} T(m-1,s,n|m,s,n) &= c\mu(1-\nu)\omega\frac{m}{K} + d\mu(1-\nu)(1-\omega)\frac{m(m-1)}{K(K-1)} \\ &\quad + \frac{1}{2}d\mu(1-\nu)(1-\omega)\frac{2ms}{K(K-1)} \\ &= \tilde{c}m + \tilde{d}m\frac{m+s}{K}, \end{aligned} \tag{B4}$$

$$\tilde{c} = \frac{c\mu(1-\nu)\omega}{K}, \tag{B5}$$

$$\tilde{d} = \frac{d\mu(1-\nu)(1-\omega)}{K-1} \approx \frac{d\mu(1-\nu)(1-\omega)}{K}, \tag{B6}$$

$$\begin{aligned} T(m,s-1,n|m,s,n) &= c\mu(1-\nu)\omega\frac{s}{K} + d\mu(1-\nu)(1-\omega)\frac{s(s-1)}{K(K-1)} \\ &\quad + \frac{1}{2}d\mu(1-\nu)(1-\omega)\frac{2ms}{K(K-1)} \\ &= \tilde{c}s + \tilde{d}s\frac{m+s}{K}, \end{aligned} \tag{B7}$$

$$T(m-1,s,n+\alpha+1|m,s,n) = e\mu\nu(1-\omega)\frac{2m(K-m-s)}{K(K-1)}\frac{n}{W} = \tilde{e}mn\left(1-\frac{m+s}{K}\right), \tag{B8}$$

$$\tilde{e} = \frac{2e\mu\nu(1-\omega)}{(K-1)W} \approx \frac{2e\mu\nu(1-\omega)}{KW}, \tag{B9}$$

$$\begin{aligned} T(m-1,s,n+\beta+1|m,s,n) &= f\mu\nu(1-\omega)\frac{m(m-1)}{K(K-1)}\frac{n}{W} + f\mu\nu(1-\omega)\frac{2ms}{K(K-1)}\frac{n}{W} \\ &= \tilde{f}mn\frac{m+2s}{K}, \end{aligned} \tag{B10}$$

$$\tilde{f} = \frac{f\mu\nu(1-\omega)}{(K-1)W} \approx \frac{f\mu\nu(1-\omega)}{KW}, \tag{B11}$$

$$\begin{aligned} T(m-1,s+1,n-1|m,s,n) &= h\mu\nu(1-\omega)\frac{2m(K-m-s)}{K(K-1)}\frac{n}{W} + k\mu\nu(1-\omega) \\ &\quad \times\frac{m(m-1)}{K(K-1)}\frac{n}{W} + k\mu\nu(1-\omega)\frac{2ms}{K(K-1)}\frac{n}{W} \\ &= \tilde{h}mn\left(1-\frac{m+s}{K}\right) + \tilde{k}mn\frac{m+2s}{K}, \end{aligned} \tag{B12}$$

$$\tilde{h} = \frac{2h\mu\nu(1-\omega)}{(K-1)W} \approx \frac{2h\mu\nu(1-\omega)}{KW}, \tag{B13}$$

$$\tilde{k} = \frac{k\mu\nu(1-\omega)}{(K-1)W} \approx \frac{k\mu\nu(1-\omega)}{KW}, \tag{B14}$$

$$T(m,s-1,n+\alpha|m,s,n) = p\mu(1-\nu)(1-\omega)\frac{2s(K-m-s)}{K(K-1)} = \tilde{p}s\left(1-\frac{m+s}{K}\right), \tag{B15}$$

$$\tilde{p} = \frac{2p\mu(1-\nu)(1-\omega)}{K-1} \approx \frac{2p\mu(1-\nu)(1-\omega)}{K}, \tag{B16}$$

$$\begin{aligned} T(m,s-1,n+\beta|m,s,n) &= q\mu(1-\nu)(1-\omega)\frac{s(s-1)}{K(K-1)} \\ &\quad + q\mu(1-\nu)(1-\omega)\frac{2ms}{K(K-1)} \\ &= \tilde{q}s\frac{2m+s}{K}, \end{aligned} \tag{B17}$$

$$\tilde{q} = \frac{q\mu(1-\nu)(1-\omega)}{K-1} \approx \frac{q\mu(1-\nu)(1-\omega)}{K}, \tag{B18}$$

$$T(m,s,n-1|m,s,n) = g(1-\mu)\nu\frac{n}{W} = \tilde{g}n, \tag{B19}$$

$$\tilde{g} = \frac{(1-\mu)\nu}{W}. \tag{B20}$$

Ignoring fluctuations and correlations, we derive the population dynamics at the mean-field level. The time evolution for population size is

$$\frac{d\langle m\rangle}{dt} = \langle T(m+1,s,n|m,s,n)\rangle - \langle T(m-1,s,n|m,s,n)\rangle - \langle T(m-1,s,n+\alpha-1|m,s,n)\rangle$$
$$- \langle T(m-1,s,n+\beta-1|m,s,n)\rangle - \langle T(m-1,s+1,n-1|m,s,n)\rangle$$
$$= (\tilde{b}+\tilde{d})\langle m\rangle\left(1-\frac{\langle m\rangle+\langle s\rangle}{K}\right) - (\tilde{c}+\tilde{d})\langle m\rangle - (\tilde{e}+\tilde{h})\langle m\rangle\langle n\rangle\left\{1-\frac{1}{K}\left[\left(1-\frac{\tilde{f}+\tilde{k}}{\tilde{e}+\tilde{h}}\right)\langle m\rangle + \left(1-2\frac{\tilde{f}+\tilde{k}}{\tilde{e}+\tilde{h}}\right)\langle s\rangle\right]\right\}, \tag{B21a}$$

$$\frac{d\langle s\rangle}{dt} = \langle T(m,s+1,n|m,s,n)\rangle - \langle T(m,s-1,n|m,s,n)\rangle + \langle T(m-1,s+1,n-1|m,s,n)\rangle$$
$$- \langle T(m,s-1,n+\alpha|m,s,n)\rangle - \langle T(m,s-1,n+\beta|m,s,n)\rangle$$
$$= (\tilde{b}+\tilde{d})\langle s\rangle\left(1-\frac{\langle m\rangle+\langle s\rangle}{K}\right) - (\tilde{c}+\tilde{d})\langle s\rangle - \tilde{h}\langle m\rangle\langle n\rangle$$
$$\times\left\{1-\frac{1}{K}\left[\left(1-\frac{\tilde{k}}{\tilde{h}}\right)\langle m\rangle + \left(1-2\frac{\tilde{k}}{\tilde{h}}\right)\langle s\rangle\right]\right\} - \tilde{p}\langle s\rangle\left\{1-\frac{1}{K}\left[\left(1-2\frac{\tilde{q}}{\tilde{p}}\right)\langle m\rangle + \left(1-\frac{\tilde{q}}{\tilde{p}}\right)\langle s\rangle\right]\right\}, \tag{B21b}$$

$$\frac{d\langle n\rangle}{dt} = (\alpha-1)\langle T(m-1,s,n+\alpha-1|m,s,n)\rangle + (\beta-1)\langle T(m-1,s,n+\beta-1|m,s,n)\rangle - \langle T(m-1,s+1,n-1|m,s,n)\rangle$$
$$+ \alpha\langle T(m,s-1,n+\alpha|m,s,n)\rangle + \beta\langle T(m,s-1,n+\beta|m,s,n)\rangle - \langle T(m,s,n-1|m,s,n)\rangle$$
$$= [(\alpha-1)\tilde{e}-\tilde{h}]\langle m\rangle\langle n\rangle\left\{1-\frac{1}{K}\left[\left(1-\frac{(\beta-1)\tilde{f}-\tilde{k}}{(\alpha-1)\tilde{e}-\tilde{h}}\right)\langle m\rangle + \left(1-2\frac{(\beta-1)\tilde{f}-\tilde{k}}{(\alpha-1)\tilde{e}-\tilde{h}}\right)\langle s\rangle\right]\right\}$$
$$+ \alpha\tilde{p}\langle s\rangle\left\{1-\frac{1}{K}\left[\left(1-2\frac{\beta\tilde{q}}{\alpha\tilde{p}}\right)\langle m\rangle + \left(1-\frac{\beta\tilde{q}}{\alpha\tilde{p}}\right)\langle s\rangle\right]\right\} - \tilde{g}\langle n\rangle. \tag{B21c}$$

Letting

$$r = \tilde{b}+\tilde{d}, \tag{B22a}$$
$$d_1 = \tilde{c}+\tilde{d}, \tag{B22b}$$
$$d_2 = \tilde{p}, \tag{B22c}$$
$$d_3 = \tilde{g}, \tag{B22d}$$
$$\phi_1 = \tilde{e}+\tilde{h}, \tag{B22e}$$
$$\phi_2 = \tilde{h}, \tag{B22f}$$
$$a_1 = \frac{\tilde{f}+\tilde{k}}{\tilde{e}+\tilde{h}}, \tag{B22g}$$
$$a_{21} = \frac{\tilde{k}}{\tilde{h}}, \tag{B22h}$$
$$a_{22} = \frac{\tilde{q}}{\tilde{p}}, \tag{B22i}$$
$$a_{31} = \frac{(\beta-1)\tilde{f}-\tilde{k}}{(\alpha-1)\tilde{e}-\tilde{h}}, \tag{B22j}$$
$$a_{32} = \frac{\beta\tilde{q}}{\alpha\tilde{p}}, \tag{B22k}$$

which are Eqs. (29), and omitting angular brackets for simplicity, Eqs. (B21) can be written as Eqs. (28).

[1] R. Maranger and D. Bird, Mar. Ecol.: Prog. Ser. **121**, 217 (1995).
[2] S. Chibani-Chennoufi, A. Bruttin, M.-L. Dillmann, and H. Brüssow, J. Bacteriol. **186**, 3677 (2004).
[3] C. Santelli, B. Orcutt, E. Banning, W. Bach, C. Moyer, M. Sogin, H. Staudigel, and K. Edwards, Nature (London) **453**, 653 (2008).
[4] A. Ortmann and C. Suttle, Deep-Sea Res., Part I **52**, 1515 (2005).
[5] P. G. Falkowski, T. Fenchel, and E. F. Delong, Science **320**, 1034 (2008).
[6] M. Syvanen, Annu. Rev. Genet. **28**, 237 (1994).
[7] H. Ochman *et al.*, Nature (London) **405**, 299 (2000).
[8] S. Wilhelm and C. Suttle, BioScience **49**, 781 (1999).
[9] C. Suttle, Nature (London) **437**, 356 (2005).
[10] M. Weinbauer and F. Rassoulzadegan, Environ. Microbiol. **6**, 1 (2003).
[11] S. Sharma, Z. Szele, R. Schilling, J. Munch, and M. Schloter, Appl. Environ. Microbiol. **72**, 2148 (2006).
[12] R. Monson, D. Lipson, S. Burns, A. Turnipseed, A. Delany, M. Williams, and S. Schmidt, Nature (London) **439**, 711 (2006).
[13] J. Schimel, T. Balser, and M. Wallenstein, Ecology **88**, 1386 (2007).
[14] C. A. Suttle, Nat. Rev. Microbiol. **5**, 801 (2007).
[15] R. Danovaro, A. Dell, C. Corinaldesi, M. Magagnini, R. Noble, C. Tamburini, and M. Weinbauer, Nature (London) **454**, 1084 (2008).
[16] R. Bardgett, C. Freeman, and N. Ostle, ISME J. **2**, 805 (2008).
[17] F. Rohwer and R. V. Thurber, Nature (London) **459**, 207 (2009).
[18] J. Paul, ISME J. **2**, 579 (2008).
[19] S. Sonea, Nature (London) **331**, 216 (1988).
[20] M. Sullivan, D. Lindell, J. Lee, L. Thompson, J. Bielawski, and S. Chisholm, PLoS Biol. **4**, e234 (2006).
[21] N. Goldenfeld and C. Woese, Nature (London) **445**, 369 (2007).
[22] E. S. Anderson, Nature (London) **209**, 637 (1966).
[23] N. G. Anderson, Nature (London) **227**, 1346 (1970).
[24] J. Filee, P. Forterre, and J. Laurent, Res. Microbiol. **154**, 237 (2003).
[25] D. Lindell *et al.*, Nature (London) **449**, 83 (2007).
[26] C. Pal, M. Macia, A. Oliver, I. Schachar, and A. Buckling, Nature (London) **450**, 1079 (2007).
[27] H. Hadas, M. Einav, I. Fishov, and A. Zaritsky, Microbiology **143**, 179 (1997).
[28] S. Williamson, L. Houchin, L. McDaniel, and J. Paul, Appl. Environ. Microbiol. **68**, 4307 (2002).
[29] H. Brüssow, C. Canchaya, and W.-D. Hardt, Microbiol. Mol. Biol. Rev. **68**, 560 (2004).
[30] S. Williamson and J. Paul, Aquat. Microb. Ecol. **36**, 9 (2004).
[31] H. Brüssow, Microbiology **151**, 2133 (2005).
[32] M. Rosvall, I. B. Dodd, S. Krishna, and K. Sneppen, Phys. Rev. E **74**, 066105 (2006).
[33] S. Williamson, S. Cary, K. Williamson, R. Helton, S. Bench, D. Winget, and K. Wommack, ISME J. **2**, 1112 (2008).
[34] J. Weitz, Microbe **3**, 171 (2008).
[35] A. Wallace, Annals and Magazine of Natural History, 2nd Series, **16**, 184 (1855).
[36] K. Ibrahim, R. Nichols, and G. Hewitt, Heredity **77**, 282 (1996).
[37] O. Hallatschek and D. Nelson, Theor Popul. Biol. **73**, 158 (2008).
[38] O. Hallatschek and K. S. Korolev, Phys. Rev. Lett. **103**, 108103 (2009).
[39] K. S. Korolev, M. Avlund, O. Hallatschek, and D. R. Nelson, Rev. Mod. Phys. **82**, 1691 (2010).
[40] A. J. McKane and T. J. Newman, Phys. Rev. E **70**, 041902 (2004).
[41] T. Butler and N. Goldenfeld, Phys. Rev. E **80**, 030902(R) (2009).
[42] A. Babic, A. Lindner, M. Vulic, E. Stewart, and M. Radman, Science **319**, 1533 (2008).
[43] T. Yoshida, S. Ellner, L. Jones, B. Bohannan, R. Lenski, and N. Hairston, Jr., PLoS Biol. **5**, e235 (2007).
[44] N. Held and R. Whitaker, Environ. Microbiol. **11**, 457 (2009).
[45] R. Lenski and R. May, J. Theor. Biol. **169**, 253 (1994).
[46] A. Koch, Virology Journal **4**, 121 (2007).
[47] D. Refardt and P. Rainey, Evolution **64**, 1086 (2009).
[48] M. Ptashne, *A Genetic Switch: Phage Lambda Revisited* (CSHL Press, New York, 2004).
[49] K. Bæk, S. Svenningsen, H. Eisen, K. Sneppen, and S. Brown, J. Mol. Biol. **334**, 363 (2003).
[50] B. Levin, F. Stewart, and L. Chao, Am. Nat. **111**, 3 (1977).
[51] I. Wang, D. Dykhuizen, and L. Slobodkin, Evol. Ecol. **10**, 545 (1996).
[52] B. Bohannan and R. Lenski, Ecology **78**, 2303 (1997).
[53] E. Beretta and Y. Kuang, Nonlinear Anal.: Real World Appl. **2**, 35 (2001).
[54] J. Fort and V. Méndez, Phys. Rev. Lett. **89**, 178101 (2002).
[55] J. Weitz, H. Hartman, and S. Levin, Proc. Natl. Acad. Sci. U.S.A. **102**, 9535 (2005).
[56] J. Weitz and J. Dushoff, Theoretical Ecology **1**, 13 (2008).
[57] M. Middelboe, Microb. Ecol. **40**, 114 (2000).
[58] C. Brussaard, J. Eukaryot Microbiol. **51**, 125 (2004).
[59] S. Sillankorva, R. Oliveira, M. Vieira, I. Sutherland, and J. Azeredo, FEMS Microbiol. Lett. **241**, 13 (2004).
[60] J. Smith, *Models in Ecology* (Cambridge University Press, Cambridge, England, 1978).
[61] T. Butler and D. Reynolds, Phys. Rev. E **79**, 032901 (2009).
[62] M. De Paepe and F. Taddei, PLoS Biol. **4**, e193 (2006).
[63] Y. Chen, I. Golding, S. Sawai, L. Guo, and E. Cox, PLoS Biol. **3**, 1276 (2005).
[64] N. Chia, I. Golding, and N. Goldenfeld, Phys. Rev. E **80**, 030901(R) (2009).
[65] R. May, Science **177**, 900 (1972).
[66] A. Kolmogorov, Iyal. Attuary **7**, 74 (1936).
[67] D. Gillespie, J. Comput. Phys. **22**, 403 (1976).
[68] D. Gillespie, J. Phys. Chem. **81**, 2340 (1977).
[69] A. Marr, Microbiol. Mol. Biol. Rev. **55**, 316 (1991).
[70] M. Middelboe, A. Hagström, N. Blackburn, B. Sinn, U. Fischer, N. Borch, J. Pinhassi, K. Simu, and M. Lorenz, Microb. Ecol. **42**, 395 (2001).
[71] E. Aurell, S. Brown, J. Johanson, and K. Sneppen, Phys. Rev. E **65**, 051914 (2002).
[72] P. Kourilsky, Virology **45**, 853 (1971).
[73] S. Jiang and J. Paul, Microb. Ecol. **35**, 235 (1998).
[74] A. Kropinski and R. Warren, J. Gen. Virol. **6**, 85 (1970).
[75] C. Jepson and J. March, Vaccine **22**, 2413 (2004).